# A Multi-Frame Fractional Fourier Transform Technique for Moving Target Detection with Space-Based Passive Radar

Zhongyu Li [12], Fabrizio Santi [2*], Debora Pastina [2], Pierfrancesco Lombardo [2]

[1] School of Electronic Engineering, University of Electronic Science and Technology of China, No.2006 Xiyuan Ave West Hi-Tech Zone, Chengdu, China
[2] DIET Department, University of Rome "La Sapienza", Via Eudossiana18, Rome, Italy
[*] santi@diet.uniroma1.it

**Abstract:** This paper puts forward a moving target detection technique for space-based passive radar. The main drawback of satellite transmitters for radar applications is the very low power density on the ground level, which requires long integration times to adequately increase the signal to background ratio. To this aim, in this paper a new technique is proposed relying on a hybrid coherent/non-coherent integration of the received signal in the Fractional Fourier Transform (FrFT) domain. After the compensation of the range walk by Keystone reformatting, a coherent integration is performed over consecutive short time intervals (frames) such that the coherence of the scattering mechanism within each frame can be assumed. Then, a proper combination of the multiple frames is performed based on the kernel of the FrFT, allowing the reliable detection of low observable targets. The effectiveness of the proposed technique has been proved by simulated analysis considering very low EIRP satellites as opportunity transmitters.

## 1. Introduction

Space-borne passive radar systems are a very promising alternative to conventional systems relying on dedicated transmitters. The lack of dedicated transmitters allows low cost operations and, since the system is intrinsically bistatic, it represents an effective anti-stealth defense option. With respect to terrestrial transmitters, satellites can provide a wider accessibility on the global scale, and new generations of satellites (e.g. the European navigation satellite system Galileo) are encouraging developments of emerging technologies for remote sensing applications [1]. A number of studies and experiments have been conducted over the last years exploiting communications and navigation satellites, mainly addressing the imaging of stationary scenes [2]-[7], whereas a very limited number of studies concern the case of moving objects [1],[8],[9]. In this work, we put forward a novel surface moving target detection technique for a passive radar system involving a ground-based stationary receiver and a satellite opportunistic transmitter.

The proposed technique is based on the Fractional Fourier Transform (FrFT), which has been studied intensively in the past years by the radar community, with application at moving target detection [10], imaging [11]-[13], beamforming [14] and waveform generation [15]. With specific regard to moving target detection, the moving target echo can be generally regarded as a chirp signal, and the FrFT can concentrate its energy in the Doppler Centroid (DC) – Doppler Frequency Rate (DFR) domain, where the moving target can be isolated from the stationary contribution [10].

In the large majority of the FrFT-based moving target detection techniques, the coherent integration gain provided by the selection of a proper rotation angle of the transform kernel suffices to make the energy of the moving target echo high enough to compete with the noise and clutter levels [16][17]. However, satellite transmitters provide a very low level of the power density on the ground level, and the processing interval should be increased up to several tens of seconds to strengthen the target's energy sufficiently. As an example, in [8] it has been demonstrated that a coherent processing interval (CPI) of 30 s is needed to achieve a signal-to-noise ratio (SNR) value of 12 dB for a target with 10 $m^2$ radar cross section (RCS) 40 km away from the receiver referring to a geostationary transmitter from the Eutelsat fleet. The situation can be even worst in the GNSS case considering the lower EIRP level [9],[18]. However, when the integration time increases, the range migration occurs, entailing significant worsening of the integration performance. Some innovative techniques have been proposed to enlarge the CPI in the case of range cell migration, such as the Generalized Radon Fourier Transform [19] and the Radon Fractional Fourier Transform [20]. Nevertheless, they have been considered for active radar systems, where the transmitted power is such that CPIs in the order of few seconds suffice for the detection of low observable targets.

For the space-based passive radar systems under consideration, reaching suitable values of SNRs requires longer dwell times, and the coherent integration is no more feasible because the scattering mechanism cannot be regarded as coherent. Therefore, a hybrid coherent/non-coherent integration technique is here proposed. By segmentation of the data received during the aperture time in short time intervals, the FrFT can be efficiently applied to each frame allowing to transit in the DC-DFR domain. To further increase the SNR, the single-frame DC-DFR maps are non-coherently combined. However, the target position will change in both range and Doppler position, and therefore the single frame maps cannot be directly integrated. Therefore, a proper combination strategy has to be defined. As will be detailed later, Keystone reformatting is exploited to align the single frame data in the range dimension, whereas in the DC dimension the alignment of the individual frame maps is driven by the kernel of the FrFT. A simulated analysis considering very low EIRP satellites is then provided, showing the effectiveness of the proposed technique to increase the detection performance of the space-based passive radar system.

The paper is organized as follows: Section II describes the echo model and Section III the proposed multi-frame technique. Simulated results are shown in Section IV and some conclusions in Section V close the paper.

## 2. Echo Model

The acquisition geometry of the considered satellite-based passive radar is shown in Fig. 1 referring to a maritime application. $T_x$ is the satellite opportunistic transmitter, $R_x$ the ground based stationary receiver, $R_b$ the baseline between $T_x$-$R_x$, $R_t$ and $R_r$ are the distances between the moving target and respectively $T_x$ and $R_x$. Due to the motion of the target, with speed $V$ and direction $\theta$ (measured with respect to the Rx line-of-sight, LOS), as well as the possible motion of $T_x$, above distances change with time.

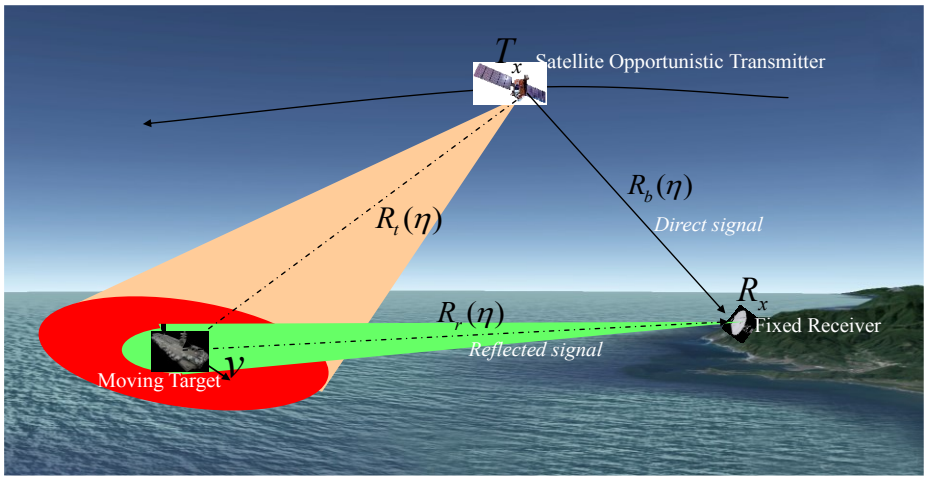


***Fig. 1.*** *Operative scenario*

The receiver has two co-located antennas: the reference antenna steered toward $T_x$ acquiring the direct signal (reference signal for matched filter) and the surveillance antenna acquiring the reflected signal from the area to be surveyed. After range compression, the signal from the moving target in range-compressed data in the fast-time&slow-time $(\tau, \eta)$ domain can be modeled as follows:

$$rr(\tau,\eta) = \sigma_\eta rect\left[\frac{\eta}{T_s}\right] exp\left\{-j\frac{2\pi}{\lambda}[R_t(\eta) + R_r(\eta) - R_b(\eta)]\right\} \times \rho\left[\tau - \frac{R_t(\eta)+R_r(\eta)-R_b(\eta)}{c}\right] \quad (1)$$

where $\rho(\tau)$ is the cross-correlation function between reflected and the reference signal, which shape depends on the particular satellite transmitter, $\lambda$ denotes the carrier wavelength, $rect(\cdot)$ selects the time window of the received signal, $T_s$ is the available observation time on the target and finally $\sigma_\eta$ denotes the complex reflectivity of the target possibly changing with slow-time $\eta$. Expanding the differential bistatic range history into second-order Taylor series, we get

$$rr(\tau,\eta) = \sigma_\eta rect\left[\frac{\eta}{T_s}\right] exp\left\{-j\frac{2\pi}{\lambda}[R_0 + A\eta + 0.5B\eta^2]\right\} \times \rho\left[\tau - \frac{R_0+A\eta+0.5B\eta^2}{c}\right] \quad (2)$$

where $R_0 = R_t(0) + R_r(0) - R_b(0)$, $A = -\lambda f_{dc}$, $B = -\lambda f_{dr}$ being $f_{dc}$ and $f_{dr}$ respectively the DC and DFR of the target.

As expected, from (2) we observe that target motion gives rise to both range and Doppler migration. Taking into account the long integration times needed for the application under consideration, both migrations should be tackled and compensated to recover SNR values suitable for detection: this is the aim of the processing technique derived in the following section

## 3. Moving Target Detection Technique

The block diagram of the proposed integration technique is sketched in Fig. 2: the overall chain comprises three stages described in detail in the following.

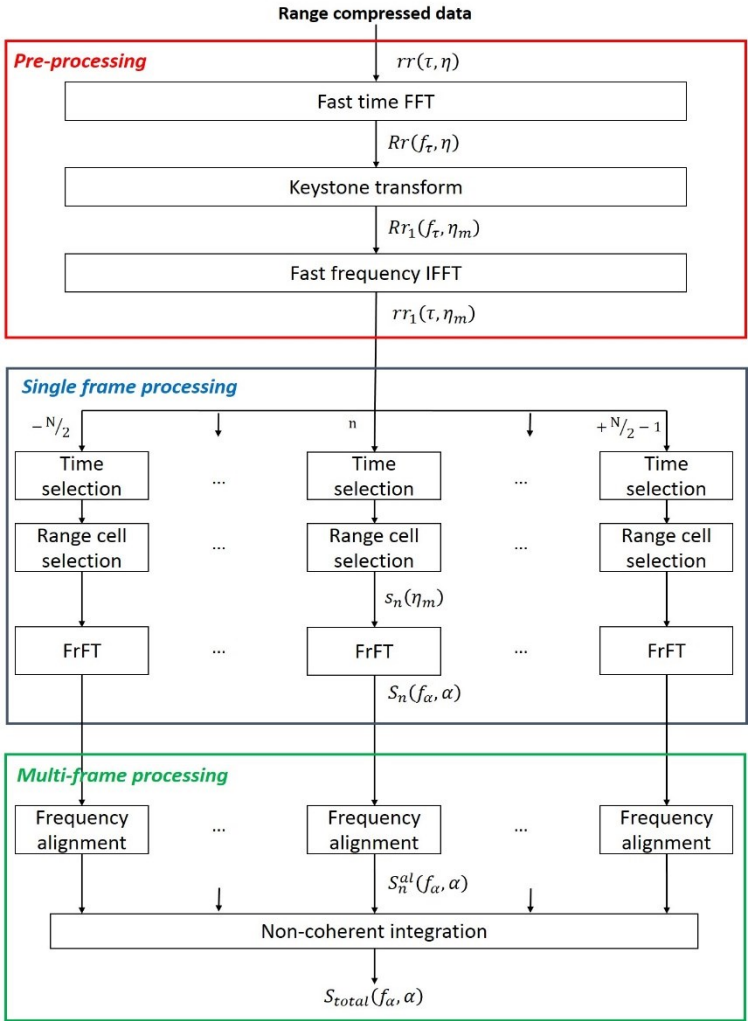


***Fig. 2.*** *Integration technique block diagram.*

### *3.1. Pre-processing*

The pre-processing stage aims at correcting the range cell migration (RCM) in the range compressed data so that the following stages can perform integration on the slow-time domain. Particularly, in the proposed technique, RCM compensation is obtained by using the Keystone Transform (KT): to this purpose

- the range compressed signal (2) is Fourier transformed to go in the range-frequency&slow-time domain, i.e. $Rr(f_\tau, \eta)$;
- the first order KT is applied, [21], thus obtaining

$$Rr_1(f_\tau, \eta_m) = Rr\left(f_\tau, \eta = \frac{f_c}{f_\tau + f_c}\eta_m\right) \quad (3)$$

where $\eta_m$ is the new azimuth time after the KT;

- the RCM corrected data are obtained after inverse Fourier transform as follows

$$rr_1(\tau, \eta_m) = \sigma_{\eta_m} rect\left[\frac{\eta_m}{T_s}\right] exp\left\{-j\frac{2\pi}{\lambda}\left[R_0 + A\eta_m + \frac{B}{2}\eta_m^2\right]\right\} \times \rho\left(\tau - \frac{R_0}{c}\right) = s_a(\eta_m) \times \rho\left(\tau - \frac{R_0}{c}\right) \quad (4)$$

being $s_a(\eta_m)$ the azimuth signal concerning range gate at range $R_0$. The above procedure, making use of the first-order KT, allows the removal of the coupling effects of the linear RCM, but they continue to exist in the quadratic order terms. However, taking into account the coarse range resolution provided by the systems under consideration, the effect of such higher-order RCM is expected to be smaller than one range resolution cell and therefore has been ignored in deriving (4). From (4), we observe that most of the moving target's energy is now gathered in a single range gate. This is the foundation of the following processing.

### *3.2. Single Frame Processing*

Considering the fluctuations of the RCS over the long integration time, the RCM corrected data are divided into multiple frames, each frame corresponding to a specific slow-time interval. Let $K$ be the number of range cells corresponding to the area of interest: for the $k$th range cell the FrFT is applied to each individual frame to go in the DC-DFR domain, where the moving target can be isolated from the disturbance contributions and the SNR can be increased. Each frame has a length of few seconds so that it is reasonable to assume the RCS fluctuations limited.

For the sake of clearness, the ensuing description on single frame processing is restricted to azimuth signal only, i.e. $s_a(\eta_m)$ in (4). First the azimuth signal is divided into $N$-frames, i.e.,

$$s_n(\eta_m) = \sigma_n rect\left[\frac{\eta_m - n \cdot T_f}{T_f}\right] exp\left\{-j\frac{2\pi}{\lambda}\left[R_0 + A\eta_m + \frac{B}{2}\eta_m^2\right]\right\} \quad (5)$$

where $n = -N/2, \ldots, 0, \ldots, N/2 - 1$, $T_f = T_s/N$ is the frame length and the variation of $\sigma_n$ inside the frame is supposed to be limited and thus is neglected.

For each frame the corresponding signal $s_n(\eta_m)$ is transformed into a rotated time axis $\mu$ as follows [10]

$$s_{n\alpha}(\mu) = \begin{cases} \sqrt{\frac{1-jcot\alpha}{2\pi}} e^{j\frac{\mu^2}{2}cot\alpha} \int_{-\infty}^{\infty} s_n(\eta_m) \\ \times e^{j\frac{\eta_m^2}{2}cot\alpha} \times e^{j\mu\eta_m csc\alpha} d\eta_m, & if \quad \alpha \neq q\pi \\ s_n(\eta_m) & if \quad \alpha = 2q\pi \\ s_n(-\eta_m) & if \quad \alpha = (2q+1)\pi \end{cases} \tag{6}$$

where $\alpha$ is the rotation angle and $q$ is integer. Then the FrFT is obtained by Fourier transforming with respect to $\mu$

$$S_n(f_\alpha, \alpha) = FFT[s_{n\alpha}(\mu)] \tag{7}$$

being $f_\alpha$ the rotated frequency after FrFT.

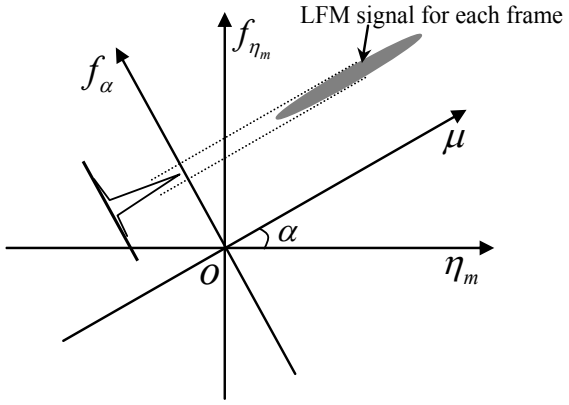


***Fig. 3.*** *Projection of LFM signal onto FrFT domain.*

Fig. 3 shows the well-known projection of a linear frequency modulated (LFM) signal onto the FrFT domain, [10]; basically the time-frequency distribution of the signal is projected onto a rotated frequency axis $f_\alpha$ with a proper angle $\alpha$ so that the energy distribution of the chirp can be highly concentrated in this FrFT domain, i.e. provides a peak in the position $(f_\alpha^*, \alpha^*)$ depending on the $(A,B)$ values. As a consequence, the Doppler centroid and Doppler frequency rate associated to the LFM signal (and thus to the target) can be easily retrieved in such FrFT plane as

$$f_{dc} = \frac{f_{\alpha^*}}{cos(\alpha^*)} \quad \& f_{dr} = tan(\alpha^*)\frac{PRF}{T_f} \tag{8}$$

being *PRF* the equivalent pulse repetition frequency of the system.

For high-EIRP geostationary satellites and/or large RCS targets, the coherent integration accomplished by the FrFT in (8) should be sufficient for the target detection. However, for low EIRP sources and/or low-RCS targets, this coherent integration is not sufficient. To counteract this problem, a proper non-coherent

combination of the DC-DFR maps coming from the multiple frames can be applied in order to reach proper SNR values enabling target detection.

### *3.3. Multi- Frames Processing*

Since different frames pertain to different observation times, the moving target will be differently located in the FrFT planes arising from the multiple frames: this implies that a proper alignment procedure is needed to enable non-coherent integration of the maps. On this basis:

- the *n*th frame is aligned to the reference frame (here assumed to be the $n = 0$ frame) thus obtaining the *n*th aligned map $S_n^{al}(f_\alpha, \alpha)$ with $n = -N/2 \dots N/2 - 1$;
- the $N$ aligned frames are non-coherently integrated thus providing

$$S_{total}(f_\alpha, \alpha) = \frac{1}{N}\sum_n \|S_n^{al}(f_\alpha, \alpha)\| \tag{9}$$

The technique here proposed for frame alignment (first step above) is based on the assumption that a given mover maintains the same DFR (i.e. $\alpha$ value) while changes its DC while changing the considered frame. This implies that a generic mover located in $(f_\alpha^*, \alpha^*)$ in the reference frame will be Doppler shifted of the amount

$$\Delta f_\alpha^n(\alpha^*) = n \times tan(\alpha^*) PRF \tag{10}$$

when observed in the *n*th frame. Therefore, the alignment can be obtained by applying an $\alpha$ dependent Doppler shift compensation, namely

$$S_n^{al}(f_\alpha, \alpha) = S_n(f_\alpha - \Delta f_\alpha^n(\alpha), \alpha) \tag{11}$$

being $\Delta f_\alpha^n(\alpha)$ coincident with (10) with $\alpha$ varying in the FrFT plane. At this point the presence of possible movers can be sought in the $S_{total}$ integrated map where the target are likely isolated from the background and therefore detectable thanks to the recovery of suitable signal to background power ratio values as shown in the following section.

## 4. Simulated Results

The effectiveness of the proposed technique is demonstrated in this section via simulations. To analyze the capability of the technique at detecting moving targets, a very demanding situation has been considered, accounting for a GPS satellite as opportunity transmitter. Navigation satellites indeed irradiate a very low power, and the power density on the ground level is around $3 \times 10^{-14}$ W/m$^2$ [18], requiring long dwell times on target.

In a first analysis, we consider a single ship target moving with $V = 10$ kt and $\theta = 45°$. At the reference instant, the ship is at 1 km from the receiver location, which collects the reflected signal for 60 s. By the tracking of the parameters of the direct signal recorded by the reference channel, i.e. time-delay, Doppler and phase, a reference signal can be locally generated and exploited to perform the range compression of the surveillance channel data, with equivalent $PRF = 1$ kHz [5], [22]. After such a signal synchronization, residual time-delay and Doppler related to the target trajectory can be retrieved by the proposed technique. For illustration, here we refer to the absence of disturbance background. Fig. 4(a) shows the range-compressed/slow-time data. As it is apparent, the range profiles are shifted during the observation time, which constitutes an obstacle to the integration performance of the long stream of data. By means of the KT, range walk can be eliminated, and the energy of the target is gathered in the same range cell over the whole aperture time. In this regard, it should be pointed out that in the analysis we considered the C/A code transmitted on the L1 channel of a GPS satellite, having a chip-rate of 1.023 MHz and therefore resulting in a bistatic range cell of about 171 m. Therefore, by correcting the linear migration the energy is well concentrated in a single range cell for a long time interval (see Fig. 4(b)).

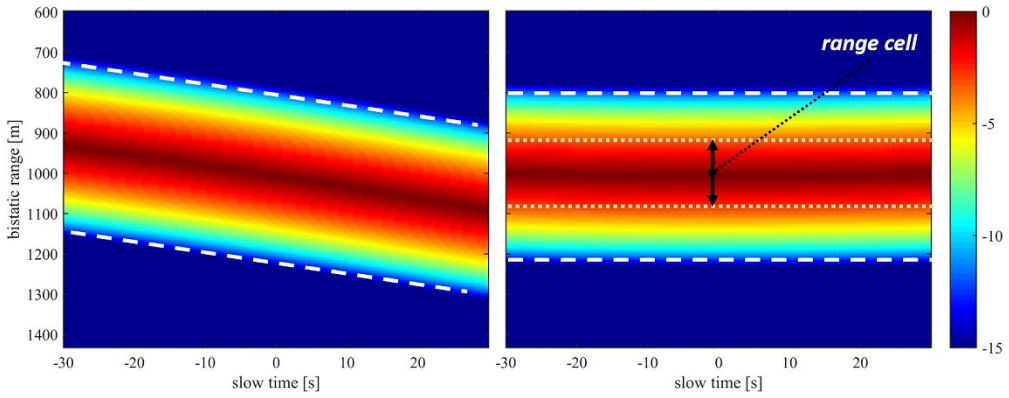


***Fig. 4.*** *Range compressed data*
a before Keystone transform
b after Keystone transform

The overall aperture time is divided in 30 frames ($T_f = 2$s), and for each range cell under test and for each frame, the FrFT is applied. The results for the range cell containing the target are shown in Fig. 5. Fig. 5(a) shows the DC-DFR surface obtained when the FrFT is applied against the central frame. It is possible to observe that the energy is concentrated along a small slice in the Doppler direction, whereas it spreads along several DFR cells, because of the short CPI along with the low velocity of the ship target. Obviously, considering faster targets, higher impact of the quadratic term of the phase in (5) is expected, and increased capability of the FrFT to concentrate the signal energy in the DFR direction would be achieved. Fig. 5(b)

and Fig. 5(c) show the results of the non-coherent combination of the multiple frames. In particular, Fig. 5(b) refers to the result obtained by directly integrating the single-frame maps, i.e. skipping the frequency alignment step in Fig. 2. Since the target is changing its position during the aperture time, it locates on different DC cells in the different frames, resulting in the blurring effect that can be observed in the figure. Fig. 5(c) shows the result obtained with the proposed technique. By applying the compensation of the DC shift in (11), the DC-DFR maps are co-registered, allowing the proper integration of the multiple frames. As it is evident looking at the figure, the signal energy is well concentrated in both the DC and DFR domain and an isolated peak can be observed. For sake of better visualization, Fig. 5(d),(e) and (f) show the corresponding two-dimensional plots.

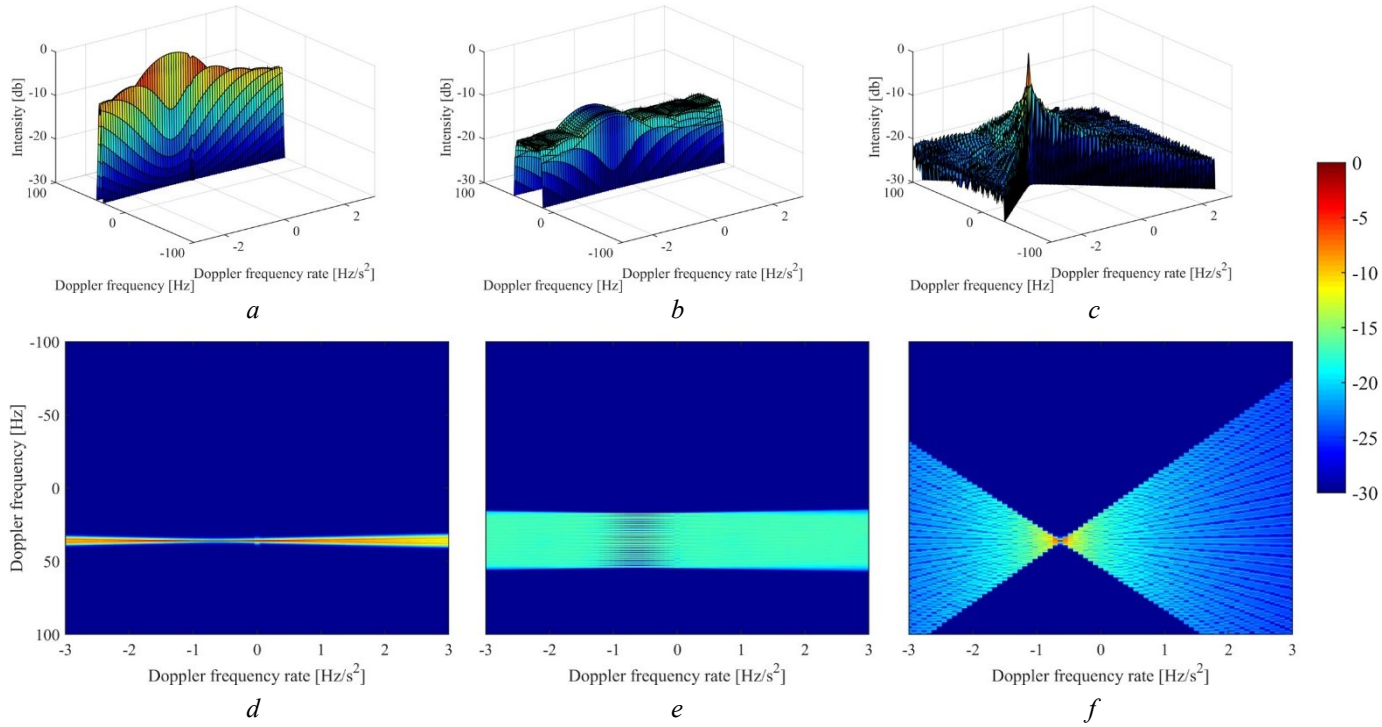


***Fig. 5.*** *Integration results in noise-free conditions*
a coherent integration over the central frame, three-dimensional plot
b non-coherent integration of multiple frames, three-dimensional plot
c non-coherent integration of multiple frames with DC-shift compensation, three-dimensional plot
d coherent integration over the central frame, two-dimensional plot
e non-coherent integration of multiple frames, two-dimensional plot
f non-coherent integration of multiple frames with DC-shift compensation, two-dimensional plot

In a second analysis, the presence of disturbance is taken into account. Particularly, an additive white Gaussian noise occupying the useful signal bandwidth is considered with noise figure 1.5 dB and noise temperature 290 K, which result in a noise power at the receiver input equal to -142 dB. Moreover, we

consider a low-cost radar receiver equipped with a small antenna with an effective area of 0.14 $m^2$, providing a limited power gain; overall 6 dB of system losses have been also taken into account. We consider the same scenario of the previous case study, and we assume the target having radar cross section of 24 dB (which could corresponds for example to a small coastal trading vessel). Fig. 6(a) shows the FrFT result concerning the range bin containing the target for the central frame. It is possible to observe that the target is buried in the noise, and it cannot be detected. Fig. 6(b) shows the result obtained by non-coherently integrating the 30 frames. Such a non-coherent integration of $N$ frames allows reducing the noise standard deviation of approximately $\sqrt{N}$. The lower variance of the noise is evident comparing Fig. 6(a) and Fig. 6(b). Specifically, we found a noise standard deviation of -106 dB in the single frame case whereas it reduces at -113 dB in the multi-frame case, accordingly to the theoretical expectations. However, since the DC shift over the different frames, the target energy is spread and therefore it cannot be detected. By applying the multi-frame combination with the proper compensation of the DC shift, the target energy increases sufficiently with respect to the noise floor and a clear peak can be observed, see Fig. 6(c). Because of the reduction of the disturbance fluctuations by means of the non-coherent integration of the several frames and the building up of the useful signal energy in the DC-DFR domain, the target could reliably be detected for example by applying a 2D CA-CFAR (Cell Averaging Constant False Alarm Rate) detector.

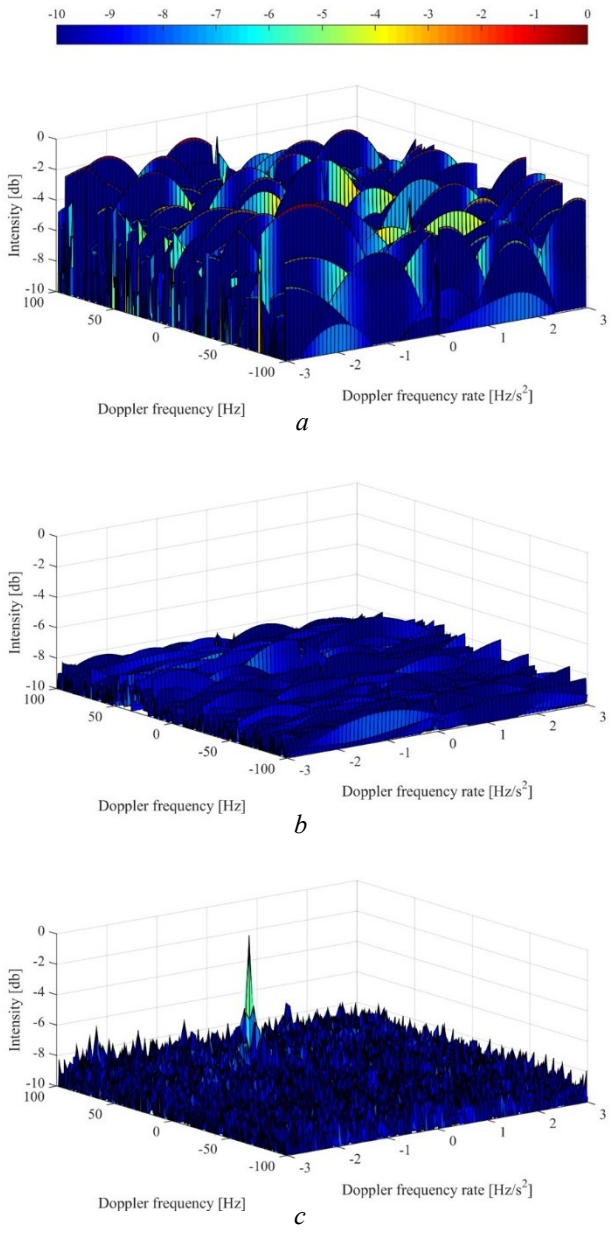


***Fig. 6.*** *Simulated case study against noise disturbance.*
a Single-frame
b Non-coherent integration of multiple frames
c Non-coherent integration of multiple frames with DC-shift compensation

So far, we considered the case of a linear target trajectory. Of course, some worsening of the technique performance are expected if target trajectory includes higher order terms. To analyze the impact of a nonlinear motion, we considered, for the same scenario of Fig. 6, a target undergoing an acceleration. Such an accelerated motion results in a residual misalignment of the DC-DFR maps concerning the different frames after the frequency alignment procedure, thus entailing a loss in terms of peak power in the final

integrated map with respect to the ideal case (i.e., the case of null acceleration). Fig. 7 shows the resulting losses for different motion conditions: $a_x$ represents the acceleration along the axis defined by the radar LOS, whereas $a_y$ denotes the acceleration along the cross direction. As it is apparent, negligible losses ($<$ 0.2 dB) have been obtained in the case of radial acceleration only. In the worst case, namely acceleration along the cross direction, a maximum loss of 3 dB has been obtained for the considered values. In this regards, it is worth to point out that if shorter integration times may be considered (for example exploiting higher EIRP sources or considering higher RCS targets), smaller losses in the case of accelerated motion can be obtained.

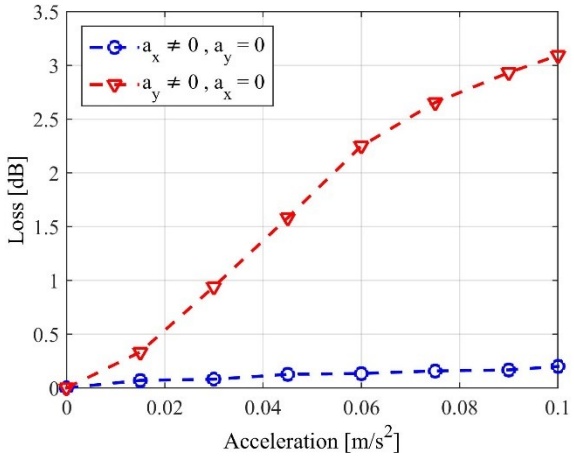


***Fig. 7.*** *Integration gain losses for targets undergoing accelerations ($T_s$ = 60s).*

Finally, the case of multiple targets has been considered. We considered two ships located in the same range cell at the reference time. The parameters of the two ships are reported in Table I. The proposed technique is applied considering a single frame duration of 2 s and an overall integration time of 60 s. The results of the multi-frame processing for the range cell containing the targets is shown in Fig. 8. We can observe that both the targets can be separately detected in the DC-DFR multi-frame map, as a consequence of i) the improvement of the SNR resulting from the proposed multi-frame processing and ii) the linearity of the FrFT operator, which does not suffer for the cross-terms when multiple targets exist. This analysis confirms the capability of the proposed multi-frame FrFT-based technique to considerably improve the detection performance of multiple low observable targets.

**Table 1** Multiple targets parameters

| Ship | Velocity | Heading angle | Radar cross section |
|---|---|---|---|
| 1 | 10 kt | 45° | 24.0 dB |
| 2 | 20 kt | 10° | 25.4 dB |

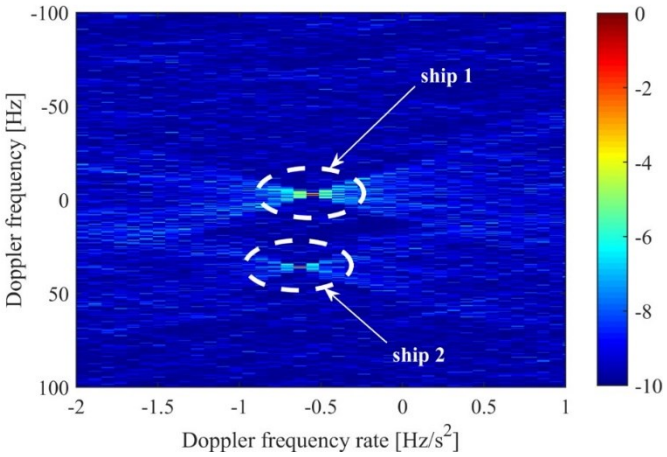


***Fig. 8.*** *Multi-frame technique in the case of two low observable targets.*

## 5. Conclusion

The paper puts forward a moving target detection technique for a space-based passive radar system, where the low power density reaching the Earth‘s surface represents the main issue. To increase the detection capability of the system, a multi-frame technique based on the FrFT is proposed. In contrast with the existing detection methods based on the FrFT, the coherent integration gain provided by a CPI limited at few seconds does not suffice to bring the signal out of the noise. Therefore, the proposed method applies the FrFT to consecutive frames of data and then performs a proper integration of the resulting DC-DFR maps. Since the target changes its position during the integration time, the technique has to handle with both range and Doppler migrations. The former issue can be resorted by Keystone reformatting applied to the whole stream of data. Then, it is analytically shown that the shift in Doppler position is linked to the kernel of the fractional transform. Therefore, a frequency alignment procedure based on the rotation angle of the transform is exploited to accomplish the Doppler alignment of the multiple frames. The non-coherent integration of the range and frequency aligned DC-DFR maps allows to increase the detection performance of the system under consideration. Simulated analysis considering very low EIRP sources demonstrates the capability of

the proposed technique to increase the detection capability of the space-based passive radar, to be exploited for example in maritime surveillance applications.

## 6. References


[1] Cristallini, D., Caruso, M., Falcone, P., *et al*.: 'Space-based passive radar enabled by the new generation of geostationary broadcast satellites', Aerospace Conference, 2010 IEEE, Big Sky, MT, 2010, pp. 1-11.

[2] Cazzani, L., Colesanti, C., Leva, D., *et al*.: 'A ground-based parasitic SAR experiment', IEEE Trans. Geosci. Remote Sens., vol. 38, no. 5, pp. 2132-2141, Sep 2000.

[3] Cherniakov, M., Kubic, K., Nezlin, D.: 'Bistatic synthetic aperture radar with non-cooperative LEOS based transmitter', Proc. of IEEE 2000 International Geoscience and Remote Sensing Symposium, Honolulu, HI, pp. 861-862, vol.2, 2000.

[4] Cherniakov, M., Saini, R., Zuo, R., Antoniou, M.: 'Space-surface bistatic synthetic aperture radar with global navigation satellite system transmitter of opportunity-experimental results', IET Radar, Sonar & Navigation, vol. 1, no. 6, pp. 447-458, Dec. 2007.

[5] Antoniou, M., Cherniakov, M.: 'GNSS-based bistatic SAR: a signal processing view', EURASIP J. Adv. Sign. Process., 2013:98.

[6] Santi, F., Antoniou, M., Pastina, D., "Point Spread Function Analysis for GNSS-Based Multistatic SAR," IEEE Geosci. Remote Sens. Lett., vol. 12, no. 2, pp. 304 – 308, Feb. 2015.

[7] Santi, F., Bucciarelli, M., Pastina, D., Antoniou, M., Cherniakov, M.: 'Spatial resolution improvement in GNSS-based SAR using multistatic acquisition and feature extraction', IEEE Trans. Geosci. Remote Sens., vol. 54, no. 10, pp. 6217-6231 Oct. 2016.

[8] Pastina, D., Sedhei, M., Cristallini, D.: 'Geostationary satellite based passive bistatic ISAR for coastal surveillance', Proc. IEEE Radar Conference, Washignton, DC, USA, May 2010.

[9] Wachtl, S., Koch V., Schmidt, L.P.: 'Global navigation satellite systems in passive surveillance applications', Tyrrhenian International Workshop on Digital Communications - Enhanced Surveillance of Aircraft and Vehicles, Rome, 2014, pp. 135-140.

[10] Sun, H.-B., Liu, G.-S., Gu, H., Su, W.-M.: 'Application of the Fractional Fourier Transform to moving target detection in airborne SAR', IEEE Trans. Aerosp. Electron. Syst., vol. 38, no. 4, pp. 1416–1424, Oct. 2002.

[11] Amein, S., Soraghan, J.J.: 'A New Chirp Scaling Algorithm Based on the Fractional Fourier Transform', IEEE Signal Process. Lett., vol. 12, no. 10, pp. 705-708, Oct. 2005.

[12] Clemente, C., Soraghan, J.J.: 'Range Doppler and chirp scaling processing of synthetic aperture radar data using the fractional Fourier transform', IET Signal Process., vol. 6, no. 5, pp. 503-510, July 2012.

[13] Pelich, R., Lonépé, N., Mercier, G., Hajduch, G., Garello, R.: 'Vessel refocusing and velocity estimation on SAR imagery using the Fractional Fourier Transform', IEEE Trans. Geosci and Remote Sens., vol. 54, no. 3, pp. 1670-1684, Mar. 2016.

[14] Samil Yetik, I., Nehorai, A.: 'Beamforming using the fractional Fourier transform', IEEE Trans. Signal Process., vol. 51, no. 6, pp. 1663-1668, June 2003.

[15] Clemente, C., Shorokhov, I., Proudler, I., Soraghan, J.J.: 'Radar waveform libraries using fractional Fourier transform', 2014 IEEE Radar Conference, Cincinnati, OH, 2014, pp. 0855-0858

[16] Guan, J., Chen, X.L., Huang, Y., He, Y.: 'Adaptive fractional Fourier transform-based detection algorithm for moving target detection in heavy sea clutter', IET Radar Sonar Navig., vol. 6, no. 5, pp. 389-401, 2012.

[17] Chen, X., Guan, J., He, Y., Zhang, J.: 'Detection of low observable moving target in sea clutter via fractal characteristics in fractional Fourier transform domain', IET Radar Sonar Navig., vol. 7, no. 6, pp. 635-651, 2013.

[18] He, X., Cherniakov, M., Long, T.: 'Signal detectability in SS-BSAR with GNSS non-cooperative transmitter', IEE Proc. Radar Sonar Navig., vol. 152, no. 3, pp. 124-132, Jun 2005.

[19] Xu, J., Yu, J., Peng, Y.-N., Xia, X.-G.: 'Radon-Fourier Transform for radar target detection, I: Generalized Doppler filter bank', IEEE Trans. Aerosp. Electron. Syst., vol. 47, no. 2, pp. 1186–1202, Apr. 2011.

[20] Chen, X., Guan, J., Liu, N., He, Y.: 'Maneuvering target detection via Radon-Fractional Fourier Transform-based long-time coherent integration', IEEE Trans. Signal Process., vol. 62, no. 4, pp. 939-953, Feb. 2014.

[21] Perry, R., Dipietro, R., Fante, R.: 'SAR imaging of moving targets', IEEE Trans. Aerosp. Electron. Syst., vol. 35, no. 1, pp. 188–200, Jan. 1999.

[22] Zeng, Z.: 'Generic signal synchronisation algorithm for passive global navigation satellite system-based synthetic aperture radar', IET Radar Sonar Navig., vol. 9, no. 4, pp. 364-373, 2015.